Compressive Near-Field Localization For Multipath RIS-aided Environments

Compressive Near-Field Localization For Multipath RIS-aided Environments

Omar Rinchi, *Member, IEEE*, Ahmed Elzanaty, *Senior, Member, IEEE*, and Mohamed-Slim Alouini, *Fellow, IEEE*

***Abstract*—Reconfigurable intelligent surfaces (RISs) are considered among the key techniques to be adopted for sixth-generation cellular networks (6G) to enhance not only communications but also localization performance. In this regard, we propose a novel single-anchor localization algorithm for a state-of-the-art architecture where the position of the user equipment (UE) is to be estimated at the base station (BS) with the aid of a RIS. We consider a practical model that accounts for both near-field propagation and multipath environments. The proposed scheme relies on a compressed sensing (CS) technique tailored to address the issues associated with near-field localization and model mismatches. Also, the RIS phases are optimized to enhance the positioning performance, achieving more than one order of magnitude gain in the localization accuracy compared to RISs with non-optimized phases.**

***Index Terms*—Reconfigurable Intelligent Surface (RIS); localization; positioning; 6G; compressed sensing; near-field;**

I. Introduction

The sixth-generation cellular networks (6G) are expected to consider higher frequency bands, wider bandwidths, and massive antenna arrays to enhance the performance of wireless communications and localization systems [1]. Some issues may arise due to considering high-frequency bands, such as the blockage of the line-of-sight (LOS) signal. In this regard, reconfigurable intelligent surfaces (RISs) has been recently introduced to alleviate this problem by providing an alternative reflective path that can be controlled [2]–[4].

In [5], the positioning performance limit of a RIS-aided single-anchor localization architecture is derived in terms of the Cramér-Rao lower bound (CRLB). Regarding positioning algorithms, the authors in [6] propose a received signal strength (RSS)-based positioning scheme. However, these works consider a far-field model, which may not be valid, especially for large RISs with high-frequencies, and hence the spherical wavefront cannot be exploited [7].

On the other hand, the authors in [8] consider the localization performance limits in RIS-aided scenarios through a model that is also valid for near-field, accounting for the position information embedded in the spherical wavefront.

Nevertheless, the aforementioned schemes do not consider multipath environments, which are typical in communications, especially indoors. In [9], a localization scheme is considered in multipath RIS-assisted environments. The complexity of this scheme is high as it relies on a maximum a posteriori (MAP) estimator, and it also considers a far-field model. To the best of the authors' knowledge, efficient localization algorithms in near-field multipath scenarios, as in indoor and/or large RIS-aided positioning, are still lacking.

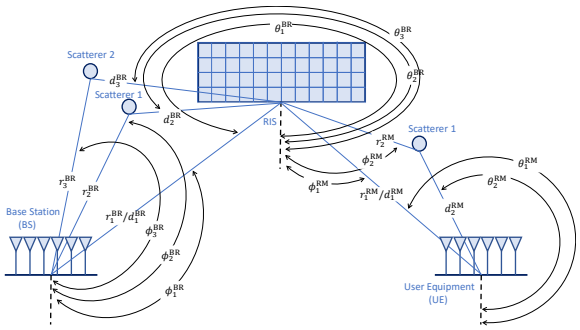

Fig. 1: The proposed architecture for RIS-aided localization.

In this paper, we propose an uplink positioning scheme where the user equipment (UE) is to be localized by a base station (BS), exploiting the beam focusing capabilities of a RIS. First, we estimate the steering angles and distances using compressed sensing (CS), accounting for the near-field multipath model. Then, we address the basis mismatch problem due to the grid-based CS. Finally, we iteratively design the RIS phases to maximize the signal-to-noise ratio (SNR), enhancing the localization performance. The main contributions can be summarized as follows.

- We propose a framework to localize a UE in a multipath near-field RIS-aided model using CS.
- We estimate the model mismatch error introduced by CS.
- We propose a RIS phase design that is based on maximizing the SNR at the BS.

Notation: Matrices will be represented by a capital bold letter $\mathbf{X}$, vectors will be denoted by bold lowercase letter $\mathbf{x}$, scalars will be represented by non-bold letter x or X, $(.)^H$, $(.)^*$ and $(.)^\dagger$ are Hermitian transpose, conjugate, and pseudo-inverse operators, diag$(.)$ is an operator that takes a vector and transforms it to a diagonal matrix, tr$(.)$ is an operator that computes the trace of a matrix, rank$(.)$ is an operator that accounts for the matrix rank, $\mathbf{I}_{N^{\mathrm{M}}}$ is an identity matrix of size N^{M}, $\mathbb{E}\{.\}$ is the expected value operator, $||.||_\ell$ is the ℓ^{th} norm, $||.||_F$ is the Frobenius norm, $\mathbf{a}_l$ represents the l^{th} column of a matrix $\mathbf{A}$, $\mathbf{a}_{b*}$ is its b^{th} row, and $a_{b,l}$ is the b^{th} element of the vector $\mathbf{a}_l$, and $\mathcal{M} \triangleq \{-M, -M+1, \cdots, M\}$ and $\mathcal{B} \triangleq \{-B, -B+1, \cdots, B\}$.

O. Rinchi is with the Department of Electrical and Computer Engineering, Missouri University of Science and Technology (e-mail: omar.rinchi@ieee.org).
A. Elzanaty is with the Institute for Communication Systems (ICS), Home of the 5G and 6G Innovation Centres (5GIC and 6GIC), University of Surrey, Guildford GU2 7XH, United Kingdom (e-mail: a.elzanaty@surrey.ac.uk).
M.-S. Alouini is with Computer, Electrical and Mathematical Sciences and Engineering (CEMSE) Division, King Abdullah University of Science and Technology (KAUST), Thuwal 23955-6900, Saudi Arabia (e-mail: slim.alouini@kaust.edu.sa).

II. System Model

In the considered system, the BS, RIS, and UE are located at $\mathbf{p}^{\mathrm{B}} = [x^{\mathrm{B}}, y^{\mathrm{B}}]$, $\mathbf{p}^{\mathrm{R}} = [x^{\mathrm{R}}, y^{\mathrm{R}}]$, and $\mathbf{p}^{\mathrm{M}} = [x^{\mathrm{M}}, y^{\mathrm{M}}]$, respectively, all are equipped with multiple-input multiple-output (MIMO) uniform linear arrays (ULAs) with number of elements $N^{\mathrm{B}}, N^{\mathrm{R}}$, and N^{M}. We consider a geometric model with L^{RM} and L^{BR} paths between the (UE and RIS) and (RIS and BS), respectively, and the LOS between the UE and the BS is blocked [10], as depicted in Fig. 1.

The received signal at the BS can be written as

$$\mathbf{Y} = \mathbf{H}\,\mathbf{X} + \mathbf{Z}, \tag{1}$$

where $\mathbf{X} \in \mathbb{C}^{N^{\mathrm{M}} \times M^{o}}$ is a positioning reference signal (PRS) containing orthogonal columns pilots having M^o sequences with power P, i.e, $\mathbf{X}\mathbf{X}^{\mathrm{H}} = \frac{P}{N^{\mathrm{M}}}\mathbf{I}_{N^{\mathrm{M}}}$, and $\mathbf{Z} \in \mathbb{C}^{N^{\mathrm{B}} \times \mathrm{M}^{o}}$ is an additive white Gaussian noise (AWGN) such that $z_{i,j} \sim \mathcal{CN}(0, \sigma_n^2)$. The matrix $\mathbf{H} \in \mathbb{C}^{N^{\mathrm{B}} \times N^{\mathrm{M}}}$ represents the overall channel between the BS and UE, and it can be expressed as

$$\mathbf{H} = \mathbf{H}^{\mathrm{BR}} \mathbf{\Omega} \mathbf{H}^{\mathrm{RM}}, \tag{2}$$

where $\mathbf{\Omega} \in \mathbb{C}^{N^{\mathrm{R}} \times N^{\mathrm{R}}}$ is a diagonal phase matrix of the RIS with diagonal $\mathbf{\Theta} \triangleq \left[\zeta_1 e^{j\theta_1}, \zeta_2 e^{j\theta_2}, \cdots, \zeta_{N^{\mathrm{R}}} e^{j\theta_{N^{\mathrm{R}}}}\right]$ that is assumed to be ideal (i.e., $\zeta_r = 1$), and $\mathbf{H}^{\mathrm{BR}} \in \mathbb{C}^{N^{\mathrm{B}} \times N^{\mathrm{R}}}$ represents the channel between the BS and RIS while $\mathbf{H}^{\mathrm{RM}} \in \mathbb{C}^{N^{\mathrm{R}} \times N^{\mathrm{M}}}$ accounts for the channel between the RIS and UE. In particular, we have

$$\mathbf{H}^{\mathrm{BR}} = \mathbf{A}(\boldsymbol{\phi}^{\mathrm{BR}}, \mathbf{r}^{\mathrm{BR}})\, \mathrm{diag}(\boldsymbol{\rho}^{\mathrm{BR}})\, \mathbf{A}^{H}(\boldsymbol{\theta}^{\mathrm{BR}}, \mathbf{d}^{\mathrm{BR}}), \tag{3}$$

where $\mathbf{A}(\boldsymbol{\phi}^{\mathrm{BR}},\ \mathbf{r}^{\mathrm{BR}}) \in \mathbb{C}^{N^{\mathrm{B}} \times L^{\mathrm{BR}}}$ and $\mathbf{A}(\boldsymbol{\theta}^{\mathrm{BR}}, \mathbf{d}^{\mathrm{BR}}) \in \mathbb{C}^{N^{\mathrm{R}} \times L^{\mathrm{BR}}}$ are steering matrices with angle of arrivals (AOAs), $\boldsymbol{\theta}^{\mathrm{BR}}$, and angle of departures (AODs), $\boldsymbol{\phi}^{\mathrm{BR}}$, while $\mathbf{r}^{\mathrm{BR}}$ and $\mathbf{d}^{\mathrm{BR}}$ represent the distances between the (BS and scatterers) and (scatterers and RIS), respectively. In the near-field, the elements of each steering matrix $\mathbf{A}$ in (3) can be approximated using the Fresnel approximation of the spherical wavefront model [11], [12] by its angle and distance as

$$a_{b,l}(\phi_l^{\mathrm{BR}}, r_l^{\mathrm{BR}}) = \exp\left(j\left[b\,\omega_l^{\mathrm{BR}} + b^2\,\gamma_l^{\mathrm{BR}}\right]\right), \tag{4}$$

where $\omega_l^{\mathrm{BR}} \triangleq f(\phi_l^{\mathrm{BR}})$ and $\gamma_l^{\mathrm{BR}} \triangleq g(\phi_l^{\mathrm{BR}}, r_l^{\mathrm{BR}})$ with

$$f(\phi) = -\frac{2\pi\delta}{\lambda}\sin(\phi), \quad g(\phi, r) = \frac{\pi\delta^2}{\lambda\, r}\cos^2(\phi), \tag{5}$$

where λ is the wavelength, δ is the distance of adjacent elements in the ULA. We take the element at the center as a reference such that the distance from the center to the element of index b is $\delta\, b$ where $b \in \mathcal{B}$ and $B \triangleq (N^{\mathrm{B}} - 1)/2$.[1] For the diagonal matrix $\mathrm{diag}(\boldsymbol{\rho}^{\mathrm{BR}}) \in \mathbb{C}^{L^{\mathrm{BR}} \times L^{\mathrm{BR}}}$, it represents the propagation gains of each path between the RIS and BS. The propagation gain of path l can be modeled as

$$\rho_l^{\mathrm{BR}} = \left(\frac{c}{4\pi(r_l^{\mathrm{BR}} + d_l^{\mathrm{BR}})f_c}\right)^{\frac{\mu}{2}} F, \tag{6}$$

where c is the speed of light, f_c is the carrier frequency, and F is a standard complex Gaussian random variable representing the fading. The channel $\mathbf{H}^{\mathrm{RM}}$ can be expressed in a similar way.

[1]Without loss of generality, we assume N^{B} to be an odd number.

III. RIS-aided localization algorithm

Our goal is to enhance the positioning performance by controlling the RIS phases. In this regard, we first estimate the geometric parameters, i.e., distances and steering angles, from the received signal using CS, and then the estimated location is used to design the RIS phases. We re-estimate the position using the optimized phases and repeat this procedure till convergence.

A. Estimation of the Localization Parameters

In near-field, due to the spherical wavefront, CS can not be directly applied on the received signal $\mathbf{Y}$. More precisely, the sparsifying basis, which is adopted to represent the sparse signal, requires gridding over both the angle and distance vectors, leading to higher computational complexity compared to the far-field case that requires gridding over only the angles.

In this regard, we propose to exploit the spatial correlation in the channel matrix $\mathbf{H}$. This allows us to decompose the two-dimensional CS problem into smaller simplified one-dimensional models, relaxing the coupling between the steering angle and distance vectors. In particular, we propose to estimate the channel and its empirical covariance matrix. Then, the measured signal in the CS model is considered as the empirically estimated covariance matrix rather than the directly received signal $\mathbf{Y}$.

More precisely, let us define $\mathbf{V}$ as the matrix containing some properly selected elements from the covariance matrix of the actual channel, i.e.,[2]

$$v_{b,m} \triangleq \mathbb{E}\left\{h_{b,m} {h_{p,n}}^*\right\} = \sum_{i=1}^{L^{\mathrm{BR}}}\sum_{k=1}^{L^{\mathrm{RM}}}\sum_{r=1}^{N^{\mathrm{R}}}\sum_{z=1}^{N^{\mathrm{R}}} \sigma_i^{\mathrm{BR}}\sigma_k^{\mathrm{RM}} e^{2jb\omega_i^{\mathrm{BR}}} e^{-j[r\alpha_i^{\mathrm{BR}} + r^2\beta_i^{\mathrm{BR}}]} e^{j[z\alpha_i^{\mathrm{BR}} + z^2\beta_i^{\mathrm{BR}}]} e^{j[r\omega_k^{\mathrm{RM}} + r^2\gamma_k^{\mathrm{RM}}]} e^{-j[z\omega_k^{\mathrm{RM}} + z^2\gamma_k^{\mathrm{RM}}]} e^{-2jm\alpha_k^{\mathrm{RM}}} e^{j\theta_r} e^{-j\theta_z}, \forall\, m \in \mathcal{M}, b \in \mathcal{B}, p = -b, n = -m, \tag{7}$$

where $\boldsymbol{\sigma}^{\mathrm{BR}}$ and $\boldsymbol{\sigma}^{\mathrm{RM}}$ contains the variance of each path, $M \triangleq (N^{\mathrm{M}} - 1)/2$, and $\alpha_k^{\mathrm{RM}} \triangleq f(\theta_k^{\mathrm{RM}})$, and $\beta_k^{\mathrm{RM}} \triangleq g(\theta_k^{\mathrm{RM}}, d_k^{\mathrm{RM}})$. The selected elements in the covariance matrix (with $p = -b$ and $n = -m$) are chosen such that the parts with γ_l^{BR}, which depends on the angles and distances, cancel out. This permits decoupling the angles and distances, as the remaining ω_l^{BR} depends only on the angle.

To be able to estimate the left-hand side of (7) one can use

$$\mathbf{V} = \hat{\mathbf{V}} - \mathbf{\Gamma}, \tag{8}$$

where $\hat{\mathbf{V}}$ is the covariance matrix of the estimated channel, and $\mathbf{\Gamma}$ is the covariance of the error in the channel estimation, such that $\Gamma_{b,m} = \mathbb{E}\{\mathbf{z}_{b*}\mathbf{x}_{m*}^H(\mathbf{z}_{-b*}\mathbf{x}_{-m*}^H)^H\} = 0$. The matrix $\hat{\mathbf{V}}$ can be ideally estimated using $\hat{v}_{b,m} = \mathbb{E}\{\hat{h}_{b,m}(\hat{h}_{-b,-m})^*\}$ but for a limited number of snapshots T we have

$$\tilde{v}_{b,m} = T^{-1}\sum_{t=1}^{T}\hat{h}_{b,m}^t(\hat{h}_{-b,-m}^t)^*, \forall\, m \in \mathcal{M}, b \in \mathcal{B}, \tag{9}$$

with $\hat{\mathbf{V}} = \tilde{\mathbf{V}} + \mathbf{\Lambda}$ where $\mathbf{\Lambda}$ is the error due to the limited number of snapshots, and $\hat{\mathbf{H}} = \mathbf{Y}\mathbf{X}^{\dagger}$ is the least square (LS) estimate of the channel. The matrix $\tilde{\mathbf{V}} \in \mathbb{C}^{B \times M}$ is written as

$$\tilde{\mathbf{V}} = \mathbf{S}^1(\boldsymbol{\phi}^{\mathrm{BR}})\mathbf{C}^1 + \mathbf{\Gamma} - \mathbf{\Lambda}. \tag{10}$$

[2]In the following, we refer to $\mathbf{V}$ as the covariance matrix, albeit it represents a part of the covariance matrix.

Each vector $\mathbf{s}_l^1(\boldsymbol{\phi}^{\text{BR}})$ in $\mathbf{S}^1(\boldsymbol{\phi}^{\text{BR}}) \in \mathbb{C}^{B\times L^{\text{BR}}}$ is expressed as

$$\mathbf{S}^1(\boldsymbol{\phi}^{\text{BR}}) = \left[e^{2jb\omega(\phi_1^{\text{BR}})}, e^{2jb\omega(\phi_2)^{\text{BR}}}, \ldots, e^{2jb\omega(\phi_{L^{\text{BR}}}^{\text{BR}})}\right]. \quad (11)$$

In (11), we defined $\mathbf{S}^1(\boldsymbol{\phi}^{\text{BR}})$ to be a combination of L^{BR} atoms each with a specific angle ϕ_l^{BR}. In order to estimate the angle $\hat{\phi}_l^{\text{BR}}$ using CS, we define the the gridded measurement matrix $\overline{\mathbf{S}}^1 \in \mathbb{C}^{B\times N}$ to be a combination of N atoms such that every single atom $\mathbf{s}_n^1(\boldsymbol{\phi}^{\text{BR}})$ is associated with the angle $\frac{2\pi n - \pi(N+1)}{N-1}$ where n is the grid counter and N is the grid size. The support matrix $\overline{\mathbf{C}}^1 \in \mathbb{C}^{N\times M}$ is L^{BR}-sparse which means that it is a matrix with N rows but only L^{BR} of them have non-zero elements and by finding the indices of the non-zero rows, one can recover the corresponding angles $\hat{\boldsymbol{\phi}}^{\text{BR}}$ up to some quantization error.

Several sparse recovery algorithms can be used to estimate the angles from the multiple measurement vectors (MMV) $\tilde{\mathbf{V}}$. For instance, the angles can be recovered by minimizing the ℓ_0 quasi-norm of $\overline{\mathbf{C}}^1$ when $B \geq 2L^{\text{BR}} + 1 - \text{rank}(\overline{\mathbf{C}}^1)$ [13], [14]. However, this problem has been shown to be NP-hard. Alternatively, the angles can be recovered using a less computationally complex optimization, i.e., ℓ_1 minimization, albeit with a higher number of measurements, e.g., $B > c\, L^{\text{BR}}$ where $c > 1$ is an overmeasuring factor [15], [16]. Several algorithms have been proposed to solve the MMV problem, e.g., multiple orthogonal matching pursuit (M-OMP), joint $\ell_{2,0}$ approximation (JLZA) and temporal multiple sparse Bayesian learning (T-MSBL), under some conditions on the restricted isometry constant of the measurement matrix $\overline{\mathbf{S}}^1$ [17]. The other angle $\hat{\boldsymbol{\theta}}^{\text{RM}}$ can be estimated by taking the Hermitian transpose of (10) and that is

$$\tilde{\mathbf{V}}^H = \mathbf{S}^2(\boldsymbol{\theta}^{\text{RM}})\mathbf{C}^2 + \boldsymbol{\Gamma}^H - \boldsymbol{\Lambda}^H. \quad (12)$$

Now by constructing the gridded measurement matrix $\overline{\mathbf{S}}^2$ similar to $\overline{\mathbf{S}}^1$, one can solve for the L^{RM} sparse support matrix $\overline{\mathbf{C}}^2 \in \mathbb{C}^{N\times B}$ using CS. To estimate the distances $\hat{\mathbf{r}}^{\text{BR}}$ that corresponds to the angle $\hat{\boldsymbol{\phi}}^{\text{BR}}$, first, we rewrite (1) as

$$\mathbf{Y} = \mathbf{A}(\boldsymbol{\phi}^{\text{BR}}, \mathbf{r}^{\text{BR}})\mathbf{C}^3 + \mathbf{Z}. \quad (13)$$

Then, we apply CS on the gridded model, where the gridded measurement matrix is $\overline{\mathbf{S}}^3 = \overline{\mathbf{A}}(\hat{\boldsymbol{\phi}}^{\text{BR}}, \overline{\mathbf{r}}^{\text{BR}})$ where $\overline{\mathbf{A}}(\hat{\boldsymbol{\phi}}^{\text{BR}}, \overline{\mathbf{r}}^{\text{BR}})$ is the steering matrix that is defined in (4), $\hat{\boldsymbol{\phi}}^{\text{BR}}$ is the previous estimated angle and $\overline{\mathbf{r}}^{\text{BR}}$ is the gridded distances vector with Fraunhofer distance being its known upper bound. Now $\hat{\mathbf{r}}^{\text{BR}}$ can be estimated using CS. The distance $\hat{\mathbf{d}}^{\text{RM}}$ can be estimated similar to $\hat{\mathbf{r}}^{\text{BR}}$ by taking the by taking the Hermitian transpose of (13) and that is

$$\mathbf{Y}^H = \mathbf{X}^H\mathbf{A}(\boldsymbol{\theta}^{\text{RM}}, \mathbf{d}^{\text{RM}})\mathbf{C}^4 + \mathbf{Z}^H. \quad (14)$$

We define the the gridded measurement matrix as $\overline{\mathbf{S}}^4 = \mathbf{X}^H\overline{\mathbf{A}}(\hat{\boldsymbol{\theta}}^{\text{RM}}, \overline{\mathbf{d}}^{\text{RM}})$ and $\hat{\mathbf{d}}^{\text{RM}}$ can be estimated similarly to all the previous parameters using CS. Similarly, the other localization parameters can be recovered.

B. Off-grid estimation

Compressed sensing considers that the angles can take only specific values on a grid with a certain resolution, leading to a model mismatch problem. Solving this problem requires an off-grid estimation, typically with high computational complexity [18]. The off-grid CS algorithms can provide higher estimation accuracy at the expense of higher computational complexity. Alternatively, we first consider on-grid CS, and then we represent the actual measurement matrix $\mathbf{S}$ as a sum of two parts: *i)* the on-grid variable $\overline{\mathbf{S}}$; *ii)* the bias mismatch error $\mathbf{E}$. For instance, to compensate for the model mismatch in (10) we can represent $\mathbf{S}^1(\boldsymbol{\phi}^{\text{BR}})$ as: $\mathbf{S}^1(\hat{\boldsymbol{\phi}}^{\text{BR}}, \boldsymbol{\phi}) \approx \mathbf{S}^1(\hat{\boldsymbol{\phi}}^{\text{BR}}) + \mathbf{S}^1_{\boldsymbol{\phi}^{\text{BR}}}(\hat{\boldsymbol{\phi}}^{\text{BR}})\text{diag}(\boldsymbol{\phi} - \hat{\boldsymbol{\phi}}^{\text{BR}})$ where $\mathbf{S}^1_{\boldsymbol{\phi}^{\text{BR}}}(\hat{\boldsymbol{\phi}}^{\text{BR}})$ is the first order derivative of $\mathbf{S}^1$ around $\hat{\boldsymbol{\phi}}^{\text{BR}}$, i.e.,

$$\mathbf{S}^1_{\boldsymbol{\phi}^{\text{BR}}}\left(\hat{\boldsymbol{\phi}}^{\text{BR}}\right) = \left[\frac{\partial \mathbf{s}_1(\phi^{\text{BR}})}{\partial \phi^{\text{BR}}}|_{\phi^{\text{BR}}=\hat{\phi}_1^{\text{BR}}}, \ldots, \frac{\partial \mathbf{s}_1(\phi^{\text{BR}})}{\partial \phi^{\text{BR}}}|_{\phi^{\text{BR}}=\hat{\phi}_{L^{\text{BR}}}^{\text{BR}}}\right]. \quad (15)$$

$\text{diag}\left(\boldsymbol{\phi} - \hat{\boldsymbol{\phi}}^{\text{BR}}\right)$ is a diagonal matrix containing the angles that minimize the mismatch error. In order to estimate, $\boldsymbol{\phi}^{\text{BR}}$ we start by solving the following optimization problem

$$\boldsymbol{\phi}^\star = \arg\min_{\boldsymbol{\phi}} ||\mathbf{S}^1(\hat{\boldsymbol{\phi}}^{\text{BR}})\hat{\mathbf{C}}^1 + \mathbf{S}^1_{\boldsymbol{\phi}^{\text{BR}}}(\hat{\boldsymbol{\phi}}^{\text{BR}})\text{diag}(\boldsymbol{\phi} - \hat{\boldsymbol{\phi}}^{\text{BR}})\hat{\mathbf{C}}^1 - \tilde{\mathbf{V}}||_F^2$$
$$\text{s.t. } -0.5\Delta \leq \phi_l - \hat{\phi}_l^{\text{BR}} \leq 0.5\Delta, \forall l \in \left\{1, 2, \cdots, L^{\text{BR}}\right\}, \quad (16)$$

where Δ is the grid resolution. Now $\boldsymbol{\phi}^{\text{BR}} \approx \tilde{\boldsymbol{\phi}}^{\text{BR}} = \hat{\boldsymbol{\phi}}^{\text{BR}} + (\boldsymbol{\phi}^\star - \hat{\phi}^{\text{BR}})$. Similarly, the off-grid errors in $\boldsymbol{\theta}^{\text{RM}}$, $\mathbf{r}^{\text{BR}}$, and $\mathbf{d}^{\text{BR}}$ can be estimated.

Algorithm 1 RIS-aided near-field positioning

Input: Y
Initialize: $\boldsymbol{\Omega} \leftarrow$ random phase design.
for $i = 1$ to I **do**
  Estimate $\tilde{\mathbf{V}}$ using (9).
  Construct the measurement matrix $\overline{\mathbf{S}}^1$ as in (11) using the required resolution.
  Estimate the $\hat{\mathbf{C}}^1$ using the sparse recovery algorithm and recover $\hat{\boldsymbol{\phi}}^{\text{BR}}$ from it.
  Compute the Hermitian transpose of $\tilde{\mathbf{V}}$ and repeat steps 4 and 5 to estimate $\hat{\boldsymbol{\theta}}^{\text{RM}}$.
  Construct the measurement matrix as in (13) using the required resolution..
  Estimate $\hat{\overline{\mathbf{C}}}^3$ using the sparse recovery algorithm and recover $\hat{\mathbf{r}}^{\text{BR}}$ from it.
  Compute the Hermitian transpose of $\mathbf{Y}$ and repeat steps 7 and 8 to estimate $\hat{\mathbf{d}}^{\text{RM}}$.
  Compute the mismatch using (16) for all the parameters.
  Use (21) to compute for $\boldsymbol{\Omega}$.
end for
Compute the UE location $\hat{\mathbf{p}}^{\text{M}}$ using (18).
Output $\hat{\mathbf{p}}^{\text{M}}$

C. Positioning

The position of the UE can be obtained from the estimated parameters, e.g., the angles and distances.[3] We consider the location of BS as the reference frame. The location of the

[3]The estimated parameters can also be used to estimate the location of scatterers, realizing simultaneous localization and mapping (SLAM).

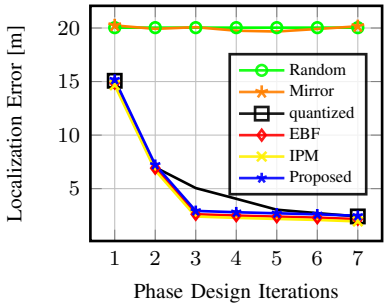

Fig. 2: Localization error for different phase design schemes.

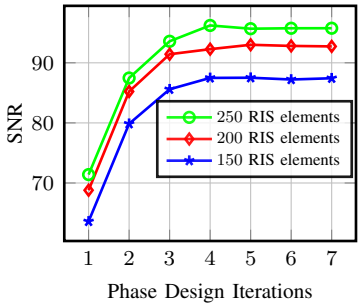

Fig. 3: SNR vs number of iterations.

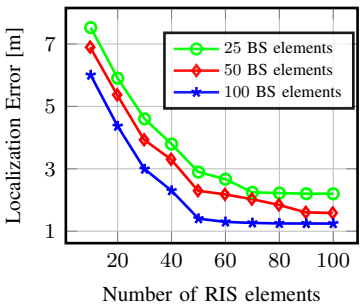

Fig. 4: Localization error vs numbers of RIS elements.

scatterers between the BS and RIS, $\mathbf{p}^{\mathrm{S,BR}} = [x^{\mathrm{S,BR}}, y^{\mathrm{S,BR}}]$, can be estimated as

$$\hat{x}_l^{\mathrm{S,BR}} = \tilde{r}_l^{\mathrm{BR}} \sin\left(\tilde{\phi}_l^{\mathrm{BR}}\right), \quad \hat{y}_l^{\mathrm{S,BR}} = -\tilde{r}_l^{\mathrm{BR}} \cos\left(\tilde{\phi}_l^{\mathrm{BR}}\right). \quad (17)$$

From each of the L^{RM} paths, we can obtain initial estimations for the UE location. The position of the UE, $\mathbf{p}^{\mathrm{M}}$, can be estimated through a weighted average of all path-based estimations as

$$\hat{x}^{\mathrm{M}} = \sum_{l=1}^{L^{\mathrm{RM}}} \nu_l \left(x^{\mathrm{R}} + \tilde{r}_l^{\mathrm{RM}} \sin\left(\tilde{\phi}_l^{\mathrm{RM}}\right) + \tilde{d}_l^{\mathrm{RM}} \sin\left(\tilde{\theta}_l^{\mathrm{RM}}\right) \right),$$
$$\hat{y}^{\mathrm{M}} = \sum_{l=1}^{L^{\mathrm{RM}}} \nu_l \left(y^{\mathrm{R}} + \tilde{r}_l^{\mathrm{RM}} \cos\left(\tilde{\phi}_l^{\mathrm{RM}}\right) - \tilde{d}_l^{\mathrm{RM}} \cos\left(\tilde{\theta}_l^{\mathrm{RM}}\right) \right), \quad (18)$$

where ν_l is the l^{th} path weight, $\sum_{l=1}^{L^{\mathrm{RM}}} \nu_l = 1$. Note that the weights ν_l of the reliable paths, e.g., the LOS path, can have higher values. Similarly, the location of the scatterers between the RIS and UE, $\mathbf{p}^{\mathrm{S,RM}} = [x^{\mathrm{S,RM}}, y^{\mathrm{S,RM}}]$, can be estimated as

$$\hat{x}_l^{\mathrm{S,RM}} = \hat{x}^{\mathrm{M}} + \tilde{d}_l^{\mathrm{RM}} \cos\left(\tilde{\theta}_l^{\mathrm{RM}}\right),$$
$$\hat{y}_l^{\mathrm{S,RM}} = \hat{y}^{\mathrm{M}} + \tilde{d}_l^{\mathrm{RM}} \sin\left(\tilde{\theta}_l^{\mathrm{RM}}\right). \quad (19)$$

D. Proposed Phase Design

The goal is to minimize the localization error by optimizing the RIS phases. Nevertheless, it is challenging to derive an analytical expression for the error. Alternatively, one can minimize the CRLB; however, the derivation of the CRLB in near-field considering reflective RIS channel with multiple scatterers is still an open problem. In this regard, we propose to maximize the SNR, as the error typically depends on it. For the SNR, it can be maximized by aiming to align the phases at the BS by minimizing the sum of the square distance of the phases from their related centroid $\bar{\epsilon}(\boldsymbol{\theta})$, i.e.,[4]

$$\boldsymbol{\theta}^{\star} = \underset{\boldsymbol{\theta}\in[0,2\pi]^{N^{\mathrm{R}}}}{\arg\min.} \sum_{b,m,i,k,r} \Big[(b\hat{\omega}_i^{\mathrm{BR}} + b^2\hat{\gamma}_i^{\mathrm{BR}}) + (r\hat{\alpha}_i^{\mathrm{BR}} + r^2\hat{\beta}_i^{\mathrm{BR}})$$
$$+ (r\hat{\omega}_k^{\mathrm{RM}} + r^2\hat{\gamma}_k^{\mathrm{RM}}) + (m\ \hat{\alpha}_k^{\mathrm{RM}} + m^2\hat{\beta}_k^{\mathrm{RM}}) + \theta_r - \bar{\epsilon}(\boldsymbol{\theta}) \Big]^2, \quad (20)$$

where $\sum_{b,m,i,k,r} \triangleq \sum_{b=-B}^{B} \sum_{m=-M}^{M} \sum_{i=1}^{L^{\mathrm{BR}}} \sum_{k=1}^{L^{\mathrm{RM}}} \sum_{r=1}^{N^{\mathrm{R}}}$, $\bar{\epsilon}(\boldsymbol{\theta})$ defined similar to [8]. Using similar techniques to [8], after some manipulations, the proposed RIS phases can be written as

$$\theta_r^{\star} = \Big((2M+1)(2B+1) L^{\mathrm{BR}} L^{\mathrm{RM}} \Big)^{-1} \sum_{b,m,i,k} \Big[b\ \hat{\omega}_i^{\mathrm{BR}}$$
$$+ b^2\hat{\gamma}_i^{\mathrm{BR}} + r\ \hat{\alpha}_i^{\mathrm{BR}} + r^2\hat{\beta}_i^{\mathrm{BR}} + r\ \hat{\omega}_k^{\mathrm{RM}} + r^2\hat{\gamma}_k^{\mathrm{RM}}$$
$$+ m\ \hat{\alpha}_k^{\mathrm{RM}} + m^2\hat{\beta}_k^{\mathrm{RM}} \Big], \forall r \in \{1, 2, \cdots, N^{\mathrm{R}}\}. \quad (21)$$

The proposed localization scheme is illustrated in Algorithm 1.

E. Computational Complexity

The proposed algorithm consists of three main steps: *i)* estimating the localization parameters using CS; *ii)* estimating the off-grid error; and *iii)* designing the RIS phases. For the first part, we consider the T-MSBL algorithm with complexity $\mathcal{O}(B^2N)$ [17]. On the other hand, the CVX [19] is considered for all other convex optimization problems. For instance, the off-grid optimization can be solved with complexity, in the worst case, of order $\mathcal{O}((L^{\mathrm{BR}})^3)$. Finally, the proposed RIS phase design is a closed-form solution with the complexity of $\mathcal{O}(N^{\mathrm{R}})$ for computing the N^{R} phases.

IV. Numerical Results

The BS, RIS, and UE are located at $\mathbf{p}^{\mathrm{B}} = [0, 0]$, $\mathbf{p}^{\mathrm{R}} = [5, 5]$, and $\mathbf{p}^{\mathrm{M}} = [10, 0]$. We assume thermal noise such that $\sigma_n^2 = B_{\mathrm{t}} T_{\mathrm{k}} K$ where $B_{\mathrm{t}} = 10$ MHz is the bandwidth, $T_{\mathrm{k}} = 290$ is the temperature in Kelvin, and K is Boltzmann constant. We set $L^{\mathrm{BR}} = 2$, $L^{\mathrm{RM}} = 2$, $f_c = 28$ GHz, $P = 1$ Watt, $N^{\mathrm{R}} = 100$, $N^{\mathrm{B}} = 51$, $N^{\mathrm{M}} = 21$, $M^{\mathrm{o}} = 60$, and $\mu = 3$, unless stated otherwise.

In Fig. 2, we show the convergence of the proposed algorithm in terms of the localization error vs the number of iterations for various phase design methodologies: *i)* proposed; *ii)* Eigen-beamforming (EBF) [20]; *iii)* random; *iv)* mirror (zero phases); *v)* 5-level quantized phases; and *vi)* optimized with interior point method (IPM). We can see that the proposed algorithm with various optimized phases can result in up to one order of magnitude reduction in the positioning error compared to non-optimized phases (i.e., Mirror and Random). Also, the proposed closed-form phase design, which does not require channel state information (CSI) knowledge, behaves as well as high computationally complex phase design methods, i.e., EBF and IPM, that require CSI knowledge.

[4] If the RIS has radio frequency chains, ρ_l^{BR} and ρ_l^{RM} can be estimated, and the amplitudes and phases of the paths can be considered in the optimization.

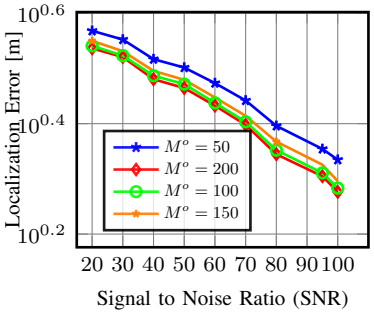

Fig. 5: Localization error for different SNR values.

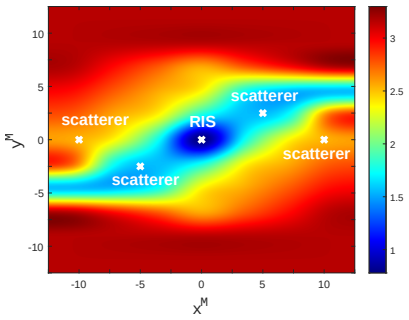

Fig. 6: Localization error for different UE locations.

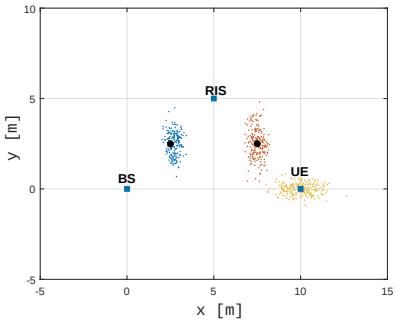

Fig. 7: SLAM performance for a multi scatterers environment.

Fig. 3 investigates the convergence of the proposed scheme in terms of the SNR. The SNR increases as the number of iterations increases till saturation after almost 4 iterations.

Fig. 4 depicts the localization error vs number of RIS elements for various numbers of BS antennas. It can be noticed that better performance can be achieved with higher number of elements, allowing the RIS to focus more power toward the BS. Also, higher number of BS antennas leads to higher number of CS measurements and better performance.

In Fig. 5, we show the impact of SNR on the localization performance by sweeping σ_n^2, for different numbers of PRS streams. The results show that the higher the SNR, the lower the localization error. Also, increasing the number of PRS streams enhances the positioning performance.

Fig. 6 represents a heat map of the localization error as a function of the UE location in the XY-plane. Here, the RIS is fixed in the location $\mathbf{p}^{\mathrm{R}} = [0, 0]$, the BS is at $\mathbf{p}^{\mathrm{B}} = [-25, -25]$, and the scatterers are located at $\mathbf{p}_1^{\mathrm{S,BR}} = [-20, 0]$, $\mathbf{p}_2^{\mathrm{S,BR}} = [-10, 5]$, $\mathbf{p}_1^{\mathrm{S,RM}} = [10, -5]$, $\mathbf{p}_2^{\mathrm{S,RM}} = [20, 0]$. The simulation shows that the error, in general, increases when the distance between the UE and RIS increases. Nevertheless, the geometry of the problem, e.g., the location of the scatterers, plays a significant role in increasing or decreasing the error. For example, the reflected signals from scatterers can be added constructively or destructively depending on their phases.

Fig. 7 shows another potential of our algorithm for simultaneous localization and mapping (SLAM) applications, where scatterers are localized along with the UE. The black dots represent the scatterers, and the colored dots are their estimated locations. We can see that the estimated location of the UE and scatters are close to the actual positions.

V. Conclusions

In this paper, we propose a RIS-aided positioning algorithm that accounts for near-field propagation and multipath environments. The algorithm relies on a CS solution that addresses both near-field and model mismatch issues. Our localization scheme can achieve more than one order of magnitude reduction in positioning error compared to non-optimized RIS phases. These results can be used to further investigate the localization capabilities of the near-field RIS-aided models, enhancing intelligent navigation and tracking systems.

References

[1] C. De Lima *et al.*, "Convergent communication, sensing and localization in 6G systems: An overview of technologies, opportunities and challenges," *IEEE Access*, vol. 9, pp. 26 902–26 925, Jan. 2021.

[2] E. Basar, M. Di Renzo, J. De Rosny, M. Debbah, M.-S. Alouini, and R. Zhang, "Wireless communications through reconfigurable intelligent surfaces," *IEEE Access*, vol. 7, pp. 116 753–116 773, Aug. 2019.

[3] A. Kafizov, A. Elzanaty, L. R. Varshney, and M.-S. Alouini, "Wireless network coding with intelligent reflecting surfaces," *IEEE Commun. Lett.*, vol. 25, no. 10, Oct. 2021.

[4] H. Ibraiwish, A. Elzanaty, Y. H. Al-Badarneh, and M.-S. Alouini, "EMF-aware cellular networks in RIS-assisted environments," *IEEE Commun. Lett.*, vol. 26, no. 1, pp. 123–127, 2021.

[5] J. He, H. Wymeersch, L. Kong, O. Silvén, and M. Juntti, "Large intelligent surface for positioning in millimeter wave MIMO systems," in *Proc. IEEE Veh. Technol. Conf. (VTC)*, Victoria, May 2020, pp. 1–5.

[6] H. Zhang, H. Zhang, B. Di, K. Bian, Z. Han, and L. Song, "MetaLocalization: Reconfigurable Intelligent Surface Aided Multi-user Wireless Indoor Localization," *IEEE Trans. Wirel. Commun.*, June 2021.

[7] A. Elzanaty, A. Guerra, F. Guidi, D. Dardari, and M.-S. Alouini, "Towards 6G Holographic Localization: Enabling Technologies and Perspectives," *arXiv preprint arXiv:2103.12415*, Mar. 2021.

[8] A. Elzanaty, A. Guerra, F. Guidi, and M.-S. Alouini, "Reconfigurable intelligent surfaces for localization: Position and orientation error bounds," *IEEE Trans. Signal Process.*, vol. 69, pp. 5386–5402, Aug. 2021.

[9] T. Ma, Y. Xiao, X. Lei, W. Xiong, and Y. Ding, "Indoor localization with reconfigurable intelligent surface," *IEEE Commun. Lett.*, vol. 25, no. 1, pp. 161–165, Sept. 2021.

[10] J. He, H. Wymeersch, and M. Juntti, "Channel estimation for RIS-aided mmWave MIMO systems via atomic norm minimization," *IEEE Trans. Wirel. Commun.*, vol. 20, no. 9, pp. 5786–5797, Apr. 2021.

[11] B. Friedlander, "Localization of signals in the near-field of an antenna array," *IEEE Trans. on Signal Process.*, vol. 67, no. 15, pp. 3885–3893, Aug. 2019.

[12] K. Hu, S. P. Chepuri, and G. Leus, "Near-field source localization using sparse recovery techniques," in *Proc. Int. Conf. Signal Process. Commun. (SPCOM)*, Bangalore, India, July 2014, pp. 1–5.

[13] A. Elzanaty, A. Giorgetti, and M. Chiani, "Weak RIC analysis of finite Gaussian matrices for joint sparse recovery," *IEEE Signal Process. Lett.*, vol. 24, no. 10, pp. 1473–1477, July 2017.

[14] ——, "Limits on sparse data acquisition: RIC analysis of finite Gaussian matrices," *IEEE Trans. Inf. Theory*, vol. 65, no. 3, Mar. 2019.

[15] J.-F. Determe, J. Louveaux, L. Jacques, and F. Horlin, "On the exact recovery condition of simultaneous orthogonal matching pursuit," *IEEE Signal Process. Lett.*, vol. 23, no. 1, pp. 164–168, Jan. 2016.

[16] D. Baron, M. B. Wakin, M. F. Duarte, S. Sarvotham, and R. G. Baraniuk, "Distributed compressed sensing," Rice University, Depart. Electrical and Computer Engineering, Tech. Rep., 2006.

[17] Z. Zhang and B. D. Rao, "Sparse signal recovery with temporally correlated source vectors using sparse bayesian learning," *IEEE J. Sel. Topics Signal Process.*, vol. 5, no. 5, pp. 912–926, June 2011.

[18] W.-G. Tang, H. Jiang, and S.-X. Pang, "Grid-free DOD and DOA estimation for MIMO radar via duality-based 2D atomic norm minimization," *IEEE Access*, vol. 7, pp. 60 827–60 836, May 2019.

[19] M. Grant, S. Boyd, and Y. Ye, "CVX: Matlab software for disciplined convex programming," 2009.

[20] H. K. Bizaki, *MIMO systems: theory and applications*. BoD–Books on Demand, 2011.